Published in final edited form as:
Nat Med. 2008 April ; 14(4): 448–453. doi:10.1038/nm1742.

Robo4 stabilizes the vascular network by inhibiting pathologic angiogenesis and endothelial hyperpermeability

Christopher A Jones[1,2,9], **Nyall R London**[1,2,9], **Haoyu Chen**[3], **Kye Won Park**[1,2,8], **Dominique Sauvaget**[4], **Rebecca A Stockton**[5], **Joshua D Wythe**[1,2], **Wonhee Suh**[2,8], **Frederic Larrieu-Lahargue**[2], **Yoh-suke Mukouyama**[6], **Per Lindblom**[4,8], **Pankaj Seth**[7], **Antonio Frias**[2], **Naoyuki Nishiya**[5,8], **Mark H Ginsberg**[5], **Holger Gerhardt**[4], **Kang Zhang**[2,3], and **Dean Y Li**[1,2]

[1]Departments of Oncological Sciences and Medicine, University of Utah, 15 North 2030 East, Salt Lake City, Utah 84112, USA.

[2]Program in Human Molecular Biology and Genetics, University of Utah, 15 North 2030 East, Salt Lake City, Utah 84112, USA.

[3]Department of Ophthalmology, University of Utah, 15 North 2030 East, Salt Lake City, Utah 84112, USA.

[4]Vascular Biology Laboratory, London Research Institute–Cancer Research UK, 44 Lincoln's Inn Fields, London WC2A 3PX, UK.

[5]Department of Medicine, University of California San Diego, 9500 Gilman Dr., La Jolla, California 92093-0726, USA.

[6]Stem Cell and Neuro-Vascular Development and Patterning Section, Laboratory of Developmental Biology, Genetics and Development Biology Center, National Heart, Lung, and Blood Institute, National Institutes of Health, Building 10, 10 Center Dr., Bethesda, Maryland 20892, USA.

[7]Renal Division and Center for Study of the Tumor Microenvironment, Department of Medicine, Beth Israel Deaconess Medical Center, Harvard Medical School, 300 Brookline Ave., Boston, Massachusetts 02215, USA.

Abstract

The angiogenic sprout has been compared to the growing axon, and indeed, many proteins direct pathfinding by both structures[1]. The Roundabout (Robo) proteins are guidance receptors with well-established functions in the nervous system2,3; however, their role in the mammalian

Correspondence should be addressed to D.Y.L. (Dean.Li@hmbg.utah.edu) or K.Z. (Kang.Zhang@hmbg.utah.edu).
[8]Present addresses: Department of Pathology and Laboratory Medicine, University of California Los Angeles, 675 Charles E. Young Dr. South, Los Angeles, California 90095, USA (K.W.P); Department of Medicine, Samsung Medical Center, Samsung Biomedical Research Institute, Sungkyunkwan University School of Medicine, 50 Ilwon-dong, Kangnam-Ku, Seoul 135-710, Korea (W.S.); Department of Microbial Chemical Biology and Drug Discovery, Iwate Medical University, School of Pharmaceutical Sciences, 2-1-1 Nishitokuda, Yahaba, Shiwa-Gun, Iwate, 028-3694, Japan (N.N.); Molecular Toxicology, Safety Assessment, AstraZeneca R&D, SE-151 85 Södertälje, Sweden (P.L.)
[9]These authors contributed equally to this work.

Note: Supplementary information is available on the Nature Medicine website.

COMPETING INTERESTS STATEMENT

The authors declare competing financial interests: details accompany the full-text HTML version of the paper at http://www.nature.com/naturemedicine/.

vasculature remains ill defined4–8. Here we show that an endothelial-specific Robo, Robo4, maintains vascular integrity. Activation of Robo4 by Slit2 inhibits vascular endothelial growth factor (VEGF)-165–induced migration, tube formation and permeability *in vitro* and VEGF-165–stimulated vascular leak *in vivo* by blocking Src family kinase activation. In mouse models of retinal and choroidal vascular disease, Slit2 inhibited angiogenesis and vascular leak, whereas deletion of *Robo4* enhanced these pathologic processes. Our results define a previously unknown function for Robo receptors in stabilizing the vasculature and suggest that activating Robo4 may have broad therapeutic application in diseases characterized by excessive angiogenesis and/or vascular leak.

To ascertain the functional significance of Robo4 *in vivo*, we generated mice in which exons one through five of the *Robo4* locus were replaced with the human placental alkaline phosphatase (*ALPP*) reporter gene (Supplementary Fig. 1a online). The resulting allele, $Robo4^{AP}$, lacks the exons encoding the immunoglobulin (IgG) repeats of the Robo4 ectodomain, which are predicted to be required for interaction with Slit proteins[9,10]. We intercrossed $Robo4^{+/AP}$ animals to generate mice that are homozygous for the targeted allele, and verified transmission of this allele by Southern blotting (Supplementary Fig. 1b). Neither *Robo4* mRNA nor Robo4 protein could be detected in $Robo4^{AP/AP}$ animals, indicating that $Robo4^{AP}$ is a null allele (Supplementary Fig. 1c and Supplementary Fig. 2a online). We also found that expression of *Robo1, Robo2* and *Robo3* and of *Slit1, Slit2* and *Slit3* is unaffected by loss of Robo4 (Supplementary Fig. 2b).

$Robo4^{AP/AP}$ animals were viable and fertile (Supplementary Table 1 online), and they showed normal patterning of the intersomitic and cephalic vessels during early embryogenesis (Supplementary Fig. 1d and Supplementary Fig. 3 online) as well as stereotypical nerve-artery alignment and smooth muscle coverage in the limb skin at embryonic day (E) 15.5 (Supplementary Fig. 4 online). These data indicated that Robo4 is not required for sprouting angiogenesis or peripheral nerve–mediated arteriogenesis in the developing mouse, and they suggested an alternate function for Robo signaling in the mammalian endothelium.

Using alkaline phosphatase activity as a marker of *Robo4* expression, we confirmed that *Robo4* is specifically transcribed in the endothelium of the developing embryo and in various vascular beds of the adult mouse (Supplementary Fig. 5 online). One vascular bed that is amenable to the analysis of developmental and pathologic angiogenesis is in the neonatal mouse retina[11–13]. High-resolution imaging of these blood vessels has demonstrated the existence of two discrete populations of endothelial cells, which possess unique structural and functional characteristics12. One population, the tip cells, are non-lumenized structures at the sprouting front of the vascular plexus that use filopodial extensions to sense and respond to extracellular cues, such as VEGF-165 (refs. 12,14). The second population, the stalk cells, form a lumenized, interconnected network that defines the remainder of the retinal vascular plexus12. To determine whether *Robo4* shows cell type–specific expression within the retinal vascular bed, we compared the expression of alkaline phosphatase to that of the pan-endothelial marker endomucin and the pericyte marker NG2. As expected, endomucin labeled the entire endothelium, and NG2 delimited the retinal vessels (Fig. 1a). Unexpectedly, we found that *Robo4* was highly transcribed in the endothelial cells that form the stalk of retinal blood vessels, and absent from many of the tip cells. We were unable to detect coincident expression of *Robo4* and NG2 in postnatal day (P) 5 and adult retinas (Fig. 1a,b); nor could we identify Robo4 in human aortic smooth muscle cells (HASMCs) by quantitative RT-PCR or western blotting (Fig. 1c,d), suggesting that Robo4 functions in an endothelial cell–autonomous fashion. The observed stalk cell–centric *Robo4* transcription was surprising given the involvement of Robo signaling in axon

guidance[2,3]. Indeed, our *a priori* hypothesis had been that *Robo4* would be strongly expressed in the tip cells, the endothelial analog of the axonal growth cone[1]. This expression pattern suggested that Robo4 has a biological role that is unrelated to the archetypal guidance mechanisms regulating vascular patterning.

Endothelial stalk cells are similar to the differentiated and stabilized phenotype characteristic of a mature, lumenized vascular tube. We hypothesized, therefore, that Robo4 expression might maintain this phenotype by inhibiting processes that are stimulated by proangiogenic factors, such as VEGF-165. Three assays routinely used to investigate angiogenesis *in vitro* assess endothelial cell proliferation, migration and tube formation, and we sought to determine the effect of Robo4 signaling on these processes. We isolated endothelial cells from the lungs of *Robo4*$^{+/+}$ and *Robo4*$^{AP/AP}$ mice and confirmed their identity through immunocytochemistry and flow cytometry (Supplementary Fig. 6 online). We then used these cells in VEGF-165–dependent proliferation, migration and tube formation assays. We found that Slit2 had no effect on VEGF-165's mitogenic activity (data not shown) but was capable of inhibiting both migration and tube formation of *Robo4*$^{+/+}$ endothelial cells (Fig. 2a,b). The inhibitory activity of Slit2 was lost in *Robo4*$^{AP/AP}$ endothelial cells, demonstrating that Slit2 inhibits endothelial cell migration and tube formation in a Robo4-dependent manner.

In a mature vascular bed, endothelial cells do not behave independently of one another; rather, they form a monolayer that prevents the movement of protein, fluid and cells from the endothelial lumen into the surrounding tissue. This barrier function can be modeled *in vitro* by using a Transwell assay to analyze the transport of a test macromolecule, such as horseradish peroxidase (HRP), across a confluent cell monolayer. Stimulation of *Robo4*$^{+/+}$ and *Robo4*$^{AP/AP}$ endothelial cells with VEGF-165, a known permeability-inducing factor, enhanced the accumulation of HRP in the lower chamber of the Transwell. Pretreatment of cell monolayers with Slit2 prevented this effect in *Robo4*$^{+/+}$, but not *Robo4*$^{AP/AP}$, endothelial cells (Fig. 2c). Next, we examined whether Slit2 had a similar influence on endothelial barrier function *in vivo* by performing a Miles assay. We injected Evans Blue into the tail vein of *Robo4*$^{+/+}$ and *Robo4*$^{AP/AP}$ mice, and subsequently injected VEGF-165 in the absence and presence of Slit2 into the dermis. The results were analogous to those of the *in vitro* assay: VEGF-165–stimulated leak of Evans Blue into the dermis could be prevented by concomitant administration of Slit2 in *Robo4*$^{+/+}$ but not *Robo4*$^{AP/AP}$ mice (Fig. 2d). We extended these observations by assessing the ability of Slit2 to suppress hyperpermeability of the retinal endothelium induced by VEGF-165. Intravitreal injection of VEGF-165 induced leak of Evans Blue from retinal blood vessels of *Robo4*$^{+/+}$ mice, which could be suppressed by co-injection of Slit2 (Fig. 2e). We repeated this experiment in the retinas of *Robo4*$^{AP/AP}$ mice and found that they were refractory to Slit2 treatment. These data demonstrated that Robo4 mediates Slit2-dependent inhibition of VEGF-165–induced endothelial hyperpermeability *in vitro* and *in vivo*.

The ability of VEGF-165 to promote angiogenesis and permeability is dependent on the activation of VEGFR2, which occurs by autophosphorylation after ligand binding[15]. Subsequently, a number of non-receptor tyrosine kinases, serine-threonine kinases and small GTPases are activated to execute VEGF-165 signaling in a spatially and temporally specific manner[15]. To determine where Slit2-Robo4 signaling intersects the VEGF-165–VEGFR2 pathway, we first analyzed VEGFR2 phosphorylation after stimulation with VEGF-165 and Slit2. Slit2 had no effect on VEGF-165–induced VEGFR2 phosphorylation (Fig. 2f), indicating that the Slit2-Robo4 pathway must intersect VEGF-165 signaling downstream of the receptor. Next, we focused our attention on the Src family of nonreceptor tyrosine kinases (SFKs)—Fyn, Yes and Src—because of their well-documented role in mediating VEGF-165–induced angiogenesis and permeability[16,17]. Treatment of endothelial cells with

Slit2 reduced VEGF-165–stimulated phosphorylation of the SFKs (Fig. 2f). Recently, several reports have shown that Src-dependent activation of the Rho family small GTPase Rac1 is essential for VEGF-165–induced endothelial cell migration and permeability[18,19]. Treatment of endothelial cell mono-layers with Slit2 prevented VEGF-165–dependent Rac1 activation (Fig. 2f). Together, these biochemical experiments suggested that the Slit2-Robo4 pathway suppresses VEGF-165–induced endothelial migration and hyperpermeability through inhibition of an SFK-Rac1 signaling axis.

We noticed that VEGF-165–stimulated *Robo4*$^{AP/AP}$ retinas had a higher rate of Evans Blue extravasation than did similarly stimulated wild-type retinas (Fig. 2e). This could result from either a basal increase in endothelial permeability or hyper-responsiveness to VEGF-165. To distinguish between these possibilities, we analyzed the extravasation of Evans Blue from *Robo4*$^{+/+}$ and *Robo4*$^{AP/AP}$ retinal vessels in the absence of stimulation with permeability-promoting factors. *Robo4*AP/AP mice showed a significant increase in Evans Blue accumulation, demonstrating that the retinal endothelium of *Robo4*$^{AP/AP}$ mice is more permeable than that of wild-type animals under basal conditions (Fig. 2g).

The ability of Robo4 signaling to block SFK activation (Fig. 2f) suggested that the basal permeability defect observed in *Robo4*$^{AP/AP}$ animals could result from excessive SFK signaling. If this were true, pharmacological suppression of SFK function in *Robo4*$^{AP/AP}$ animals should restore retinal permeability to wild-type levels. To test this idea, we injected the SFK inhibitor PP2 and its inactive analog PP3 into contralateral eyes of *Robo4*$^{+/+}$ and *Robo4*$^{AP/AP}$ mice and analyzed retinal permeability. PP2 and PP3 had no significant effect on permeability in *Robo4*$^{+/+}$ animals. However, PP2 returned the increased basal permeability in *Robo4*$^{AP/AP}$ mice to a level comparable to that observed in wild-type mice, whereas PP3 was unable to alter permeability in these animals (Fig. 2g).

In addition to Slit2, the Slit family is composed of Slit1 and Slit3 (ref. 20). All three Slit proteins interact with Robo receptors10›21 and mediate chemorepulsion of olfactory bulb explants *in vitro*[22]. There-fore, we determined whether Slit3 had the same activity as Slit2 in the assays described herein. In functional assays, we found that Slit3 blocked VEGF-165–induced Evans Blue extravasation from the retinas of *Robo4*$^{+/+}$ but not *Robo4*$^{AP/AP}$ mice; and in biochemical experiments we found that Slit3 inhibited VEGF-165–dependent SFK activation (Supplementary Fig. 7 online). Thus, several Slit family members can activate Robo4 to suppress VEGF-165–induced vascular leak.

Overexpression of Robo4 in endothelial cells, like Slit treatment, might prevent cell migration to angiogenic stimuli[7]. To test this possibility, we used adenoviral infection to overexpress Robo4 in endothelial cells. Augmented expression of Robo4, but not GFP, prevented the stimulation of cell migration and SFK phosphorylation by VEGF-165 (Supplementary Fig. 8 online). Additionally, cells infected with the Robo4 virus showed a marked reduction in basal migration and SFK phosphorylation when compared to GFP-infected cells, suggesting that tonic Robo4 signaling under basal conditions is antiangiogenic.

Vascular leak is a hallmark of the pathologic angiogenesis observed in age-related macular degeneration, retinopathy of prematurity and diabetic retinopathy. The important contribution of VEGF-165 to this process is underscored by the clinical success of antibodies to VEGF in the treatment of these diseases23›24. The demonstration that Robo4 signaling inhibits VEGF-165–dependent endothelial migration, tube formation and permeability suggests that activation of the Robo4 pathway might have clinical utility in retinal vascular disease. We used a mouse model of oxygen-induced retinopathy (OIR) that mimics the ischemia-induced angiogenesis observed in both diabetic retinopathy and

retinopathy of prematurity to investigate the effect of Robo4 signaling on retinal vascular disease. In this model, P7 mice are maintained in a 75% oxygen environment for 5 d and then returned to 25% oxygen for an additional 2 d[11]. The perceived oxygen deficit initiates a rapid increase in VEGF-165 expression in the retina, leading to increased angiogenesis and vascular leak25,26. Intravitreal administration of Slit2 markedly reduced FITC-dextran labeled retinal blood vessels in *Robo4*$^{+/+}$ but not *Robo4*$^{AP/AP}$ mice (Fig. 3a–c; arrows indicate areas of angiogenesis). Furthermore, *Robo4*$^{AP/AP}$ mice showed significantly more FITC-dextran–labeled retinal blood vessels than *Robo4*$^{+/+}$ mice after exposure to hyperoxic conditions (compare top left panels of Fig. 3a and b). In addition to FITC-dextran perfusion, we also analyzed OIR using isolectin staining and found that Slit2 treatment reduced the number of intravitreal neovascular tufts (Fig. 4a,b). Together, these data demonstrated the therapeutic potential of activating Robo4 signaling after an ischemic insult and suggested that Robo4 provides a tonic signal that stabilizes retinal blood vessels. Consistent with this notion, we found that perturbation of vascular stability in animal models of hereditary hemorrhagic telangiectasia[4] and oxygen-induced retinopathy (Supplementary Fig. 9 online) resulted in a compensatory increase in *Robo4* expression.

The increased susceptibility of *Robo4*$^{AP/AP}$ mice to oxygen-induced retinopathy suggested that endogenous Slit protein normally maintains the integrity of the retinal endothelium by acting on Robo4. If this were true, we reasoned that Slit protein would be expressed in or around the vasculature. To examine the expression of *Slit2* in the mouse retina, we performed anti-GFP immunohistochemistry on mice bearing a *GFP* gene knocked into the *Slit2* locus (*Slit2*$^{+/GFP}$ mice)[27]. GFP fluorescence was detected in cells near the retinal blood vessels of *Slit2*$^{+/GFP}$ but not *Slit2*$^{+/+}$ mice (Supplementary Fig. 10 online), demonstrating that endogenous Slit2 is available to activate Robo4 on the endothelium.

In addition to oxygen-induced retinopathy, laser-induced choroidal neovascularization, which mimics age-related macular degeneration, is commonly used to study pathologic angiogenesis in the mouse[28]. In this model, a laser is used to disrupt Bruch's membrane, which allows the underlying choroidal vasculature to penetrate into the subretinal pigment epithelium. To discern the effect of Slit2-Robo4 signaling on this pathologic process, we injected Slit2 into the eyes of 8–12-week-old mice subjected to laser-induced choroidal neovascularization. Similar to oxygen-induced retinopathy, intravitreal administration of Slit2 reduced angiogenesis in *Robo4*$^{+/+}$ mice but not *Robo4*$^{AP/AP}$ mice (Fig. 4c,d). Together, the oxygen-induced retinopathy and choroidal neovascularization models indicate that two vascular beds with distinct characteristics, one a tight blood-brain barrier and the other a fenestrated endothelium, are protected from pathologic insult by Slit2-dependent activation of Robo4 signaling.

In this report, we provide the first genetic evidence to our knowledge that Slit-Robo signaling regulates a critical function of the vasculature. We demonstrate that Robo4 is essential for Slit2-dependent inhibition of VEGF-165–induced endothelial cell migration, tube formation and hyperpermeability *in vitro* and for the moderation of angiogenesis and VEGF-165 driven hyperpermeability *in vivo*. Further, our mechanistic studies identify the SFKs as a crucial molecular target of the Slit2-Robo4 signaling axis. Collectively, these data imply that in addition to the classic paradigm of Robo receptors controlling guidance decisions in the nervous system, Slit2-dependent cues mediated by Robo4 control the integrity of the endothelium (Fig. 4e,f). The clinical success of anti-VEGF therapies in restoring vascular integrity suggests that stabilization of the mature vascular bed by activation of the Robo4 pathway may have broad therapeutic potential.

METHODS

Preparation of recombinant Slit2

COS-7 cells were transiently transfected with the empty vector pSECTAG2 or pSECTAG2::hSlit2. Forty-eight hours later, the cells were washed twice with PBS and incubated with 6 ml salt extraction buffer (10 mM HEPES, pH 7.5, 1 M NaCl and 1× complete EDTA-free protease inhibitor cocktail (Roche)) for 15 min at 25 °C. Salt extraction was repeated and the samples were centrifuged at 13,000*g* for 20 min to pellet cell debris. The supernatant was loaded on Amicon Ultra-15 concentrator columns with a 100-kDa cutoff and centrifuged until 12 ml of salt extracts was reduced to approximately 500 µl. The concentrated protein preparations were analyzed by Coomassie Blue staining and stored at 4 °C for up to 1 week. We routinely obtained Slit2 concentrations of 20–50 µg/ml. In addition to preparing concentrated protein from cells transfected with Slit2 plasmid, we performed the identical protocol on cells transfected with an empty vector (pSECTAG2). We called this preparation “Mock” and used it as a control in all experiments analyzing the effects of Slit2.

Animal models

The Institutional Animal Care and Use Committee (IACUC) at the University of Utah approved the following protocols.

Miles assay

Evans Blue was injected into the tail veins of 6–8-week-old mice, and 30 min later either saline or 10 ng of VEGF-165, each in the absence or presence of 100 ng Slit2, was injected into the dermis. After an additional 30 min, punch biopsies were performed and Evans Blue was eluted from the dermal tissue in formamide for 18 h at 60 °C. After centrifugation, the absorbance at 620 nm was measured. The amount of dermal permeability observed in saline-injected animals was set at 1. Data are presented as mean ± s.e.m. of five individual mice with each treatment in duplicate (six total injections per animal).

Retinal permeability

Retinal permeability was assessed as previously described[29]. In brief, 8–10–week-old mice were anesthetized with Avertin (2,2,2-tribromoethanol, 0.4 mg/g; Acros Organics). Mice were given an intraocular injection of 1.4 µl of 35.7 µg/ml VEGF-165 (R&D Systems) with 50 ng Slit2. An equivalent volume of Mock was injected into the contralateral eye. As indicated in Figure 2e,g, other conditions were administered. Six hours later, 50 µl of 60 mg/ml Evans Blue solution was administered via the femoral vein. After 2 h, mice were killed and perfused with citrate-buffered formaldehyde to remove intravenous Evans Blue. Eyes were enucleated and retinas dissected. Evans Blue dye was eluted in 0.4 ml formamide for 18 h at 70 °C. The extract was ultracentrifuged through a 5-kDa filter for 2 h. Absorbance at 620 nm was measured. Background absorbance was measured at 740 nm and subtracted out. Data are presented as mean ± s.e.m. of five mice per genotype.

Oxygen-induced retinopathy

OIR was induced as previously described[11]. In brief, P7 pups, along with nursing mothers, were placed in 75% oxygen. The oxygen concentration was maintained by a Pro-OX oxygen controller (Bio-Spherix). Pups were removed on P12 and given an intraocular injection of 50 ng Slit2 or Mock. Mice were sacrificed on P17 and perfused via the left ventricle with 1 ml of 50 mg/ml FITC-dextran (Sigma). Eyes were enucleated and fixed for 30 min in 4% paraformaldehyde, and retinal flat mounts were prepared. Images were taken using an Axiovert 200 fluorescence microscope (Carl Zeiss). Neovascularization per area was

quantified using AxioVision software (Carl Zeiss) to calculate the area of FITC-dextran staining. For isolectin-stained OIR samples, mice were sacrificed on P17 and their eyes enucleated and fixed for 2 h in 4% paraformaldehyde. Retinas were then dissected and stained overnight using Alexa Fluor 488–conjugated isolectin (1:50, Invitrogen). Retinal flat mounts were generated and images taken using Axiovert 200 fluorescence microscopy (Carl Zeiss). Neovascularization was quantified using AxioVision software (Carl Zeiss) to calculate the area of isolectin staining.

Laser-induced choroidal neovascularization (CNV)

2–3-month-old mice were anesthetized with Avertin and their pupils dilated with 1% tropicamide (Alcon). An Iridex OcuLight GL 532 nm laser photocoagulator (Iridex) with slit-lamp delivery system was used to create three burns three disc diameters from the optic disc at 3, 6 and 9 o'clock with the following parameters: 150 mW power, 75 μm spot size and 0.1 s duration. Production of a bubble at the time of laser treatment, indicating rupture of Bruch's membrane, is an important factor in obtaining CNV; therefore, only burns in which a bubble was produced were included in this study. Immediately after laser treatment and 3 d later, mice were given an intravitreal injection of 50 ng Slit2. An equal volume of a mock preparation was given by intravitreal injection in the other eye. One week after laser treatment, mice were sacrificed and choroidal flat mounts generated. Biotin-conjugated isolectin (Sigma) and Texas red–conjugated streptavidin (Sigma) were used to stain CNV. Flat mounts were examined using a Zeiss LSM 510 confocal microscope (Carl Zeiss) and CNV quantified using ImageJ software (NIH) to calculate the area of isolectin staining.

Statistical analyses

The Student's *t*-test or ANOVA, where appropriate, was used to assess statistical significance. A P value <0.05 was considered statistically significant.

Supplementary Material

Refer to Web version on PubMed Central for supplementary material.

Acknowledgments

We thank K. Thomas and J. Wythe for critical reading of the manuscript, L. Sorensen-Brunhart and W. Zhu for technical assistance and D. Lim for expert graphical assistance. This work was funded by grants from the US National Cancer Institute Multidisciplinary Cancer Research Training Program (N.R.L.); Cancer Research–UK (H.G.); the National Eye Institute (K.Z.); National Heart, Lung and Blood Institute (M.H.G. and D.Y.L.); and National Institute of Arthritis and Musculoskeletal and Skin Diseases (M.H.G.), the H.A. and Edna Benning Foundation, the Juvenile Diabetes Research Foundation, the American Heart Association, the Burroughs Wellcome Fund and the Flight Attendants Medical Research Institute (D.Y.L.).

References

1. Carmeliet P, Tessier-Lavigne M. Common mechanisms of nerve and blood vessel wiring. Nature 2005;436:193–200. [PubMed: 16015319]
2. Kidd T, et al. Roundabout controls axon crossing of the CNS midline and defines a novel subfamily of evolutionarily conserved guidance receptors. Cell 1998;92:205–215. [PubMed: 9458045]
3. Long H, et al. Conserved roles for Slit and Robo proteins in midline commissural axon guidance. Neuron 2004;42:213–223. [PubMed: 15091338]
4. Park KW, et al. Robo4 is a vascular-specific receptor that inhibits endothelial migration. Dev. Biol 2003;261:251–267. [PubMed: 12941633]
5. Wang B, et al. Induction of tumor angiogenesis by Slit-Robo signaling and inhibition of cancer growth by blocking Robo activity. Cancer Cell 2003;4:19–29. [PubMed: 12892710]

6. Suchting S, Heal P, Tahtis K, Stewart LM, Bicknell R. Soluble Robo4 receptor inhibits in vivo angiogenesis and endothelial cell migration. FASEB J 2005;19:121–123. [PubMed: 15486058]
7. Seth P, et al. Magic roundabout, a tumor endothelial marker: expression and signaling. Biochem. Biophys. Res. Commun 2005;332:533–541. [PubMed: 15894287]
8. Kaur S, et al. Robo4 signaling in endothelial cells implies attraction guidance mechanisms. J. Biol. Chem 2006;281:11347–11356. [PubMed: 16481322]
9. Battye R, Stevens A, Perry RL, Jacobs JR. Repellent signaling by Slit requires the leucine-rich repeats. J. Neurosci 2001;21:4290–4298. [PubMed: 11404414]
10. Howitt JA, Clout NJ, Hohenester E. Binding site for Robo receptors revealed by dissection of the leucine-rich repeat region of Slit. EMBO J 2004;23:4406–4412. [PubMed: 15496984]
11. Smith LE, et al. Oxygen-induced retinopathy in the mouse. Invest. Ophthalmol. Vis. Sci 1994;35:101–111. [PubMed: 7507904]
12. Gerhardt H, et al. VEGF guides angiogenic sprouting utilizing endothelial tip cell filopodia. J. Cell Biol 2003;161:1163–1177. [PubMed: 12810700]
13. Uemura A, Kusuhara S, Katsuta H, Nishikawa S. Angiogenesis in the mouse retina: a model system for experimental manipulation. Exp. Cell Res 2006;312:676–683. [PubMed: 16337189]
14. Ruhrberg C, et al. Spatially restricted patterning cues provided by heparin-binding VEGF-A control blood vessel branching morphogenesis. Genes Dev 2002;16:2684–2698. [PubMed: 12381667]
15. Cross MJ, Dixelius J, Matsumoto T, Claesson-Welsh L. VEGF-receptor signal transduction. Trends Biochem. Sci 2003;28:488–494. [PubMed: 13678960]
16. Eliceiri BP, et al. Src-mediated coupling of focal adhesion kinase to integrin alpha(v)beta5 in vascular endothelial growth factor signaling. J. Cell Biol 2002;157:149–160. [PubMed: 11927607]
17. Eliceiri BP, et al. Selective requirement for Src kinases during VEGF-induced angiogenesis and vascular permeability. Mol. Cell 1999;4:915–924. [PubMed: 10635317]
18. Gavard J, Gutkind JS. VEGF controls endothelial-cell permeability by promoting the β-arrestin-dependent endocytosis of VE-cadherin. Nat. Cell Biol 2006;8:1223–1234. [PubMed: 17060906]
19. Garrett TA, Van Buul JD, Burridge K. VEGF-induced Rac1 activation in endothelial cells is regulated by the guanine nucleotide exchange factor Vav2. Exp. Cell Res 2007;313:3285–3297. [PubMed: 17686471]
20. Yuan W, et al. The mouse SLIT family: secreted ligands for ROBO expressed in patterns that suggest a role in morphogenesis and axon guidance. Dev. Biol 1999;212:290–306. [PubMed: 10433822]
21. Morlot C, et al. Structural insights into the Slit-Robo complex. Proc. Natl. Acad. Sci. USA 2007;104:14923–14928. [PubMed: 17848514]
22. Patel K, et al. Slit proteins are not dominant chemorepellents for olfactory tract and spinal motor axons. Development 2001;128:5031–5037. [PubMed: 11748139]
23. Brown DM, et al. Ranibizumab versus verteporfin for neovascular age-related macular degeneration. N. Engl. J. Med 2006;355:1432–1444. [PubMed: 17021319]
24. Rosenfeld PJ, et al. Ranibizumab for neovascular age-related macular degeneration. N. Engl. J. Med 2006;355:1419–1431. [PubMed: 17021318]
25. Ozaki H, et al. Blockade of vascular endothelial cell growth factor receptor signaling is sufficient to completely prevent retinal neovascularization. Am. J. Pathol 2000;156:697–707. [PubMed: 10666398]
26. Werdich XQ, McCollum GW, Rajaratnam VS, Penn JS. Variable oxygen and retinal VEGF levels: correlation with incidence and severity of pathology in a rat model of oxygen-induced retinopathy. Exp. Eye Res 2004;79:623–630. [PubMed: 15500821]
27. Plump AS, et al. Slit1 and Slit2 cooperate to prevent premature midline crossing of retinal axons in the mouse visual system. Neuron 2002;33:219–232. [PubMed: 11804570]
28. Lima, e; Silva, R., et al. Suppression and regression of choroidal neovascularization by polyamine analogues. Invest. Ophthalmol. Vis. Sci 2005;46:3323–3330. [PubMed: 16123436]
29. Xu Q, Qaum T, Adamis AP. Sensitive blood-retinal barrier breakdown quantitation using Evans blue. Invest. Ophthalmol. Vis. Sci 2001;42:789–794. [PubMed: 11222542]

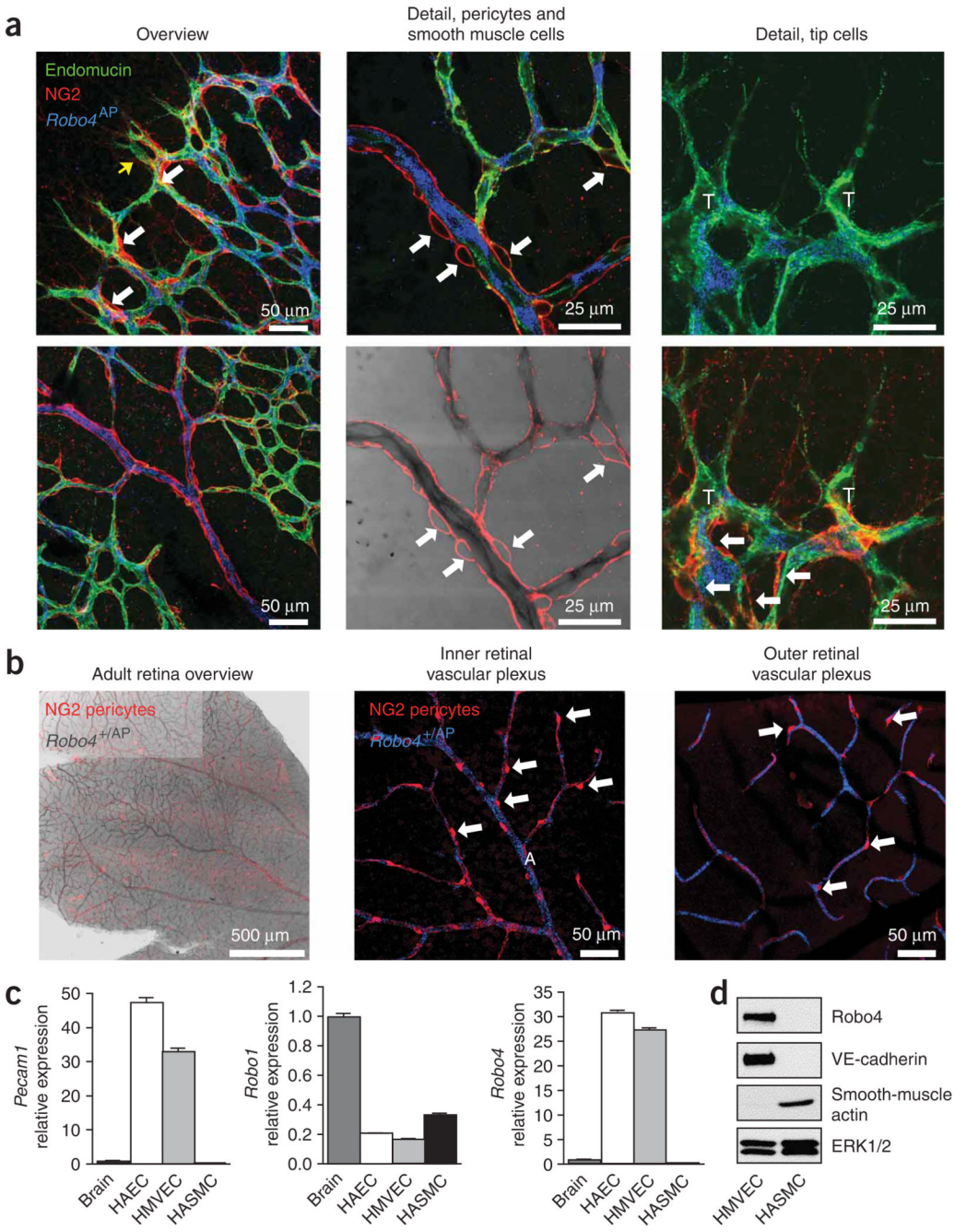

Figure 1.

Robo4 expression is endothelial specific and stalk-cell centric. (**a**) Retinal flat mounts were prepared from P5 *Robo4*$^{+/AP}$ mice and stained for endomucin (endothelial cell marker; green), NG2 (pericyte marker; red) and alkaline phosphatase (AP; *Robo4*; blue). The yellow arrow indicates a tip cell, and white arrows indicate pericytes (NG2-positive cells). T, tip cells. (**b**) Retinal flat mounts were prepared from adult *Robo4*$^{+/AP}$ mice and stained for NG2 (pericytes) and AP (*Robo4*). (**c**) Quantitative RT-PCR was performed on the indicated samples using primers specific for *Pecam1, Robo1* and *Robo4*. HAEC, human aortic endothelial cell; HASMC, human aortic smooth muscle cell; HMVEC, human microvascular endothelial cell. (**d**) Total cell lysates from HMVECs and HASMCs were

probed with antibodies to Robo4, VE-cadherin, smooth-muscle actin and ERK1/2. Experiments were performed three times and error bars represent s.e.m.

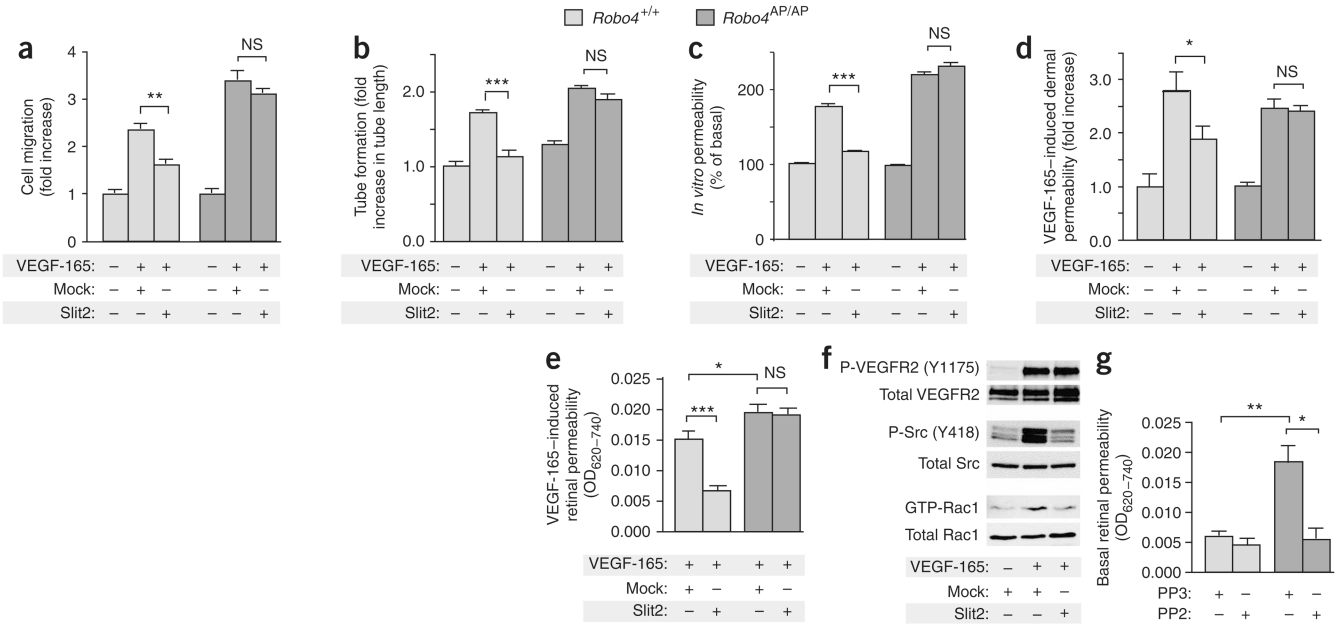

Figure 2.

Robo4 signaling inhibits VEGF-165–induced migration, tube formation, permeability and SFK activation. (**a,b**) Lung endothelial cells isolated from *Robo4*$^{+/+}$ and *Robo4*$^{AP/AP}$ mice were used in migration (**a**), tube formation (**b**) and *in vitro* permeability assays (**c**). *Robo4*$^{+/+}$ and *Robo4*$^{AP/AP}$ mice were used in the Miles assay (**d**) and retinal permeability assays (**e**). (**f**) Human microvascular endothelial cells were stimulated with VEGF-165 in the presence of Mock or Slit2 for 5 min, lysed and subjected to western blotting with antibodies to phospho-VEGFR2 (top) or phospho-Src (middle) or to Rac activation assays (bottom). (**g**) *Robo4*$^{+/+}$ and *Robo4*$^{AP/AP}$ mice were subjected to retinal permeability assays after intravitreal injection of the SFK inhibitor PP2 or the inactive analog PP3. In all panels, Mock indicates a sham preparation of Slit2. **P* < 0.05; ***P* < 0.005; ****P* < 0.0005. NS, not significant. Error bars represent s.e.m. In **a–c**, experiments were repeated three times each in triplicate. In **d, e** and **g**, five mice were tested for each condition for each genotype.

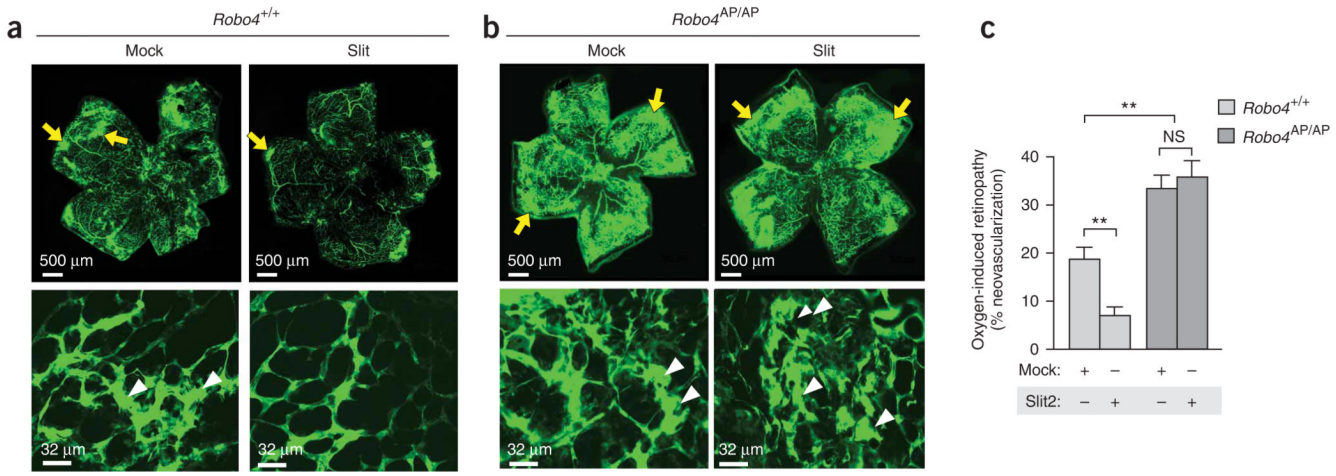

Figure 3.

Slit2 blocks oxygen-induced retinopathy in a Robo4-dependent manner. (**a,b**) Neonatal *Robo4*$^{+/+}$ (**a**) and *Robo4*$^{AP/AP}$ (**b**) mice were subjected to OIR and perfused with fluorescein isothiocyanate (FITC)-dextran (green). Retinal flat mounts were prepared for each condition and analyzed by fluorescence microscopy. Top panels are low-magnification images (yellow arrows indicate areas of increased angiogenesis), and bottom panels are high-magnification images (white arrowheads indicate neovascular tufts). (**c**) Quantification of angiogenesis observed in **a,b**. Error bars represent s.e.m. $^{**}P < 0.005$. A minimum of five mice were tested for each condition for each genotype.

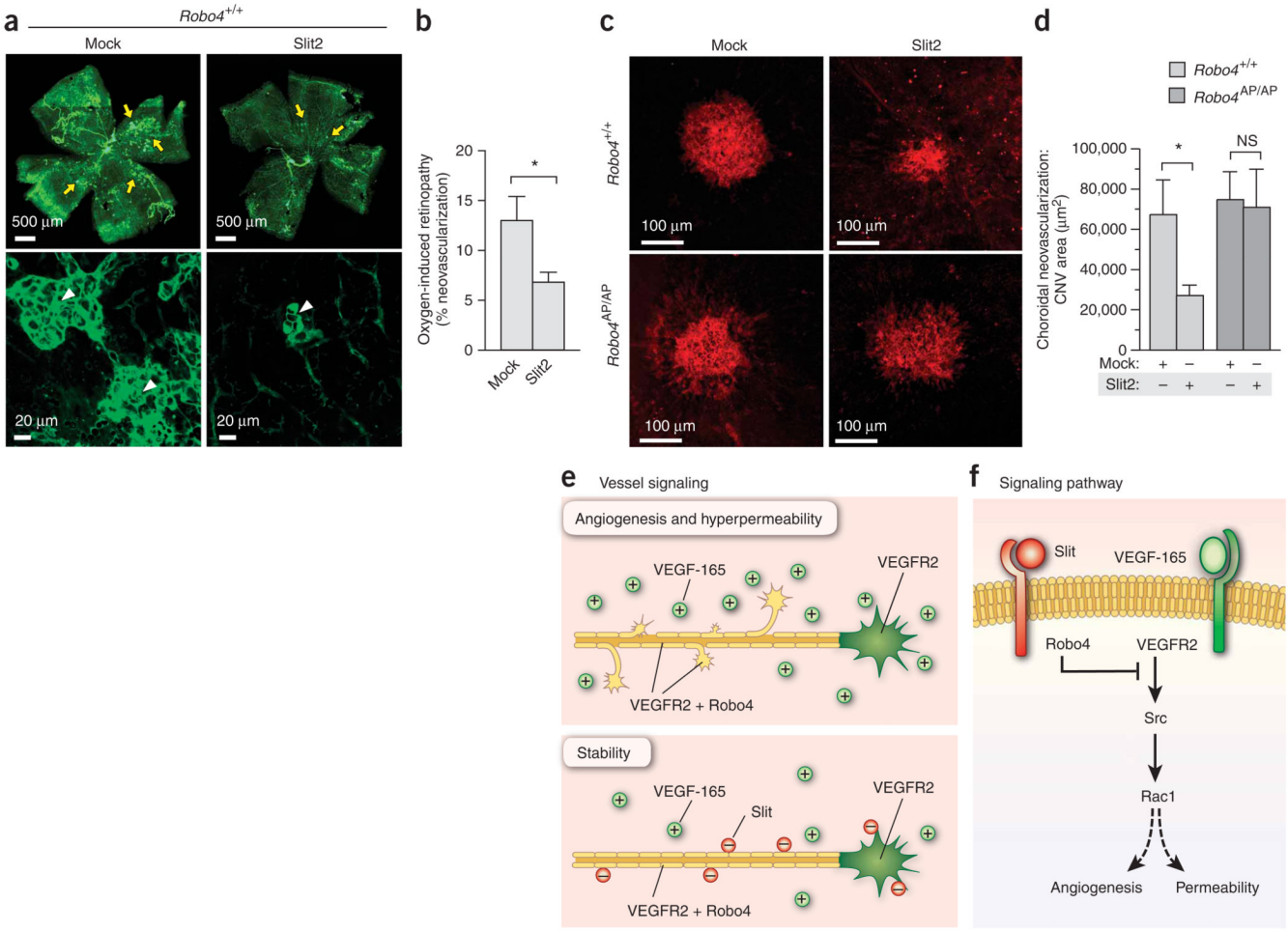

Figure 4.

Robo4 signaling inhibits pathologic angiogenesis. (**a**) Retinal flat mounts were prepared from neonatal *Robo4*$^{+/+}$ mice subjected to OIR, stained with fluorescent isolectin and analyzed by fluorescence microscopy. Top panels are low-magnification images (arrows indicate pathologic neovascular tufts), and bottom panels are high-magnification images. Arrowheads point to pathologic vascular tufts. (**b**) Quantification of pathologic neovascularization performed on a minimum of 12 mice for each condition for each genotype shown in **a**. Error bars represent s.e.m. (**c**) 2–3-month-old *Robo4*$^{+/+}$ and *Robo4*$^{AP/AP}$ mice were subjected to laser-induced choroidal neovascularization. Choroidal flat mounts were prepared, stained with fluorescent isolectin and analyzed by confocal microscopy. (**d**) Quantification of pathologic angiogenesis performed on a minimum of ten mice for each condition for each genotype shown in **c**. In all panels, Mock indicates a sham preparation of Slit2. *$P < 0.05$. NS, not significant. Error bars represent s.e.m. (**e,f**) Slit-Robo signaling promotes vascular stability via inhibition of SFKs. In the retinal endothelium, the VEGF receptor (VEGFR2) is expressed in both the tip and stalk cells, whereas Robo4 is expressed predominantly in the stalk cells (**e**). Overproduction of VEGF-165 causes angiogenesis and hyperpermeability, leading to vascular dysfunction in the retina (top). Activation of Robo4 in the stalk cells by Slit proteins limits these pathologic processes (bottom). VEGF-165 stimulates angiogenesis and permeability by activating SFKs and Rac1 in a sequential fashion[18,19] (**f**). Slit-Robo4 signaling inhibits activation of SFKs and Rac1 to block these VEGF-165–driven processes.